Geometric Study on Silicon Nanowires Fabricated via Silver-assisted Electroless Etching

Neil Irvin F. Cabello
University of the Philippines Diliman

Eloise P. Anguluan
University of the Philippines Diliman

Joseph Christopher R. Ragasa
University of the Philippines Diliman

Philippe Martin B. Tingzon*
University of the Philippines Diliman

Kerr A. Cervantes
University of the Philippines Diliman

Arvin Jay S. Escolano
University of the Philippines Diliman

Arnel A. Salvador
University of the Philippines Diliman

Armando S. Somintac
University of the Philippines Diliman

ABSTRACT

Controlling the geometry of silicon nanowires (SiNWs) has been of paramount necessity for the viability of mass-producing nanostructured devices. The length, radius, and crystallinity of SiNWs grown via one-step and two-step electroless chemical etching of p-type Si(100) in this study were controlled by varying the concentrations of etchants and etching times. Scanning electron microscope images confirmed that the length of the nanowires varied directly with increasing concentrations of HF and $AgNO_3$ for the one-step etching process, and HF, H_2O_2, and $AgNO_3$ for the two-step etching process. Diameters cannot be controlled via the electroless etching methods in the one-step process, but can be manipulated in the two-step process to some extent. X-ray diffractometry

Corresponding Author

analysis exhibited that the SiNW's peak broadening can be attributed to the slight degradation of crystallinity of SiNWs compared to bulk silicon. From the Raman spectra, SiNWs, regardless of their geometric parameters, make excellent thermo-insulators due to the one-directional movement of phonons. The slight shift in peaks can be attributed to laser heating. Finally, photoluminescence analysis of SiNWs demonstrated that the length of the SiNWs varied the ratio of the surface defects of both the one-step and two-step processes, but not the intensity.

Keywords: Nanowires (81.07.GF), silicon nanowires (78.67.Uh), silver nanoparticles (78.67.Bf)

INTRODUCTION

Studies on the nanostructure formation on the most essential and economical semiconductor available, silicon (Si), have gained a new driving force with the advent of low-cost chemical preparation of nanostructures and the approaching end of Moore's Law. Primary among these nanostructures are silicon nanowires (SiNWs), believed to be promising building blocks for the next-generation devices in the field of optoelectronics, nanoelectronics, sensing, energy storage, and harvesting.

SiNWs have a huge array of advantageous optical and optoelectronic properties. These include low thermal conductivity (Curtin et al. 2012), wide broadband optical absorption (Tsaklakos 2007), high carrier mobility (Liu et al. 2013), quantum confinement effects, and phononic properties (Bandaru and Pichanusakorn 2010). These properties are all dependent on the geometry and crystallinity of the fabricated SiNWs.

Different methods have been developed in the past years for the fabrication of SiNWs. Some commonly used techniques in the fabrication of SiNWs are the Vapor-Liquid-Solid (VLS) method (Gunawan and Guha 2009), and the chemical-assisted beam etching. However, these methods are time-consuming and make use of expensive equipment to produce the required high-vacuum environment at high temperatures for the fabrication of vertically-oriented SiNWs.

A novel technique used in the fabrication of SiNWs is silver-assisted electroless etching (EE), which has gained significant interest in the recent years (Schmidt et al. 2009), as it offers a low-cost method of fabricating vertically-aligned SiNWs using a simple table-top set-up. The process utilizes silver (Ag) which oxidizes the

Si substrate and is subsequently dissolved by an etchant solution (Peng et al. 2006). This simultaneous redox reaction and etching in the areas in contact with the noble metal forms voids in the substrate, leaving the unetched areas as SiNWs (Peng et al. 2002).

The etching process used in this study can be categorized into two types: one-step process and two-step process. One-step etching involves the immersion of the Si substrate in an etchant solution composed of hydrofluoric acid (HF) and $AgNO_3$ (Figure 1, left). The Ag+ ions in the solution are reduced and deposited as Ag nanoparticles (AgNPs) near the defective sites on top of the Si substrate are reduced by the more electronegative Si (Lin 2010) (Figure 1, right). This reduction is coupled with the oxidation of the Si beneath the AgNP and is subsequently dissolved by HF (Peng et al. 2006). The reaction is described by the following:

$$Ag^{+}+e^{-}\rightarrow Ag_{(S)} \tag{1}$$

$$Si_{(S)}+2H_2O_{(1)}SiO_2+4H^{+}+4e^{-} \tag{2}$$

Furthermore, the etching of the newly formed silicon oxide layer in the one-step process is described by the following reaction:

$$SiO_2+6HF\rightarrow H_2SiF_6+2H_2O \tag{3}$$
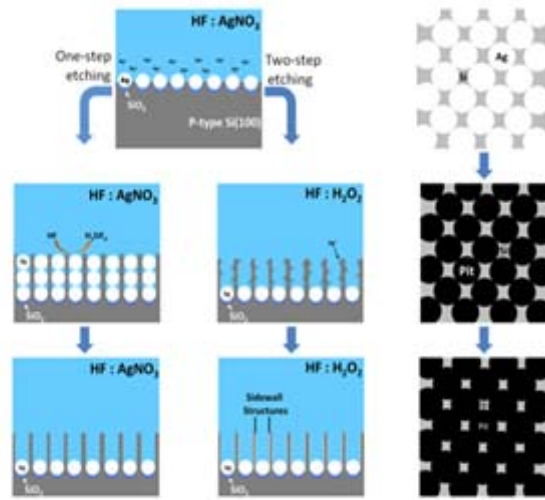
Figure 1. Etching mechanism in lateral view (left) and top view (right).

For the one-step process, the net chemical reaction using equations (1), (2), and (3) yield:

$$4Ag^+ \; Si_{(S)} + 6F^- \circledR [SiF_6]^{2-} + 4Ag_{(S)} \tag{4}$$

Meanwhile, the two-step etching process involves an additional immersion of the Si substrate in HF-hydrogen peroxide (H_2O_2) etchant solution after a prior immersion in HF-AgNO$_3$ solution (Figure 1, right). The first step deposits AgNPs onto the surface of the Si. The second step oxidizes the deposited AgNPs into Ag$^+$, which are then reduced to Ag$_{(S)}$ by injecting holes in the valence band of Si. The oxidized Si is then dissolved by HF in the etchant, which causes the etching of the substrate. The following reaction governs the two-step process:

$$Si + 2H_2O_2 + 6F^- + 4H^+ \circledR [SiF_6]^{2-} + 4H_2O \tag{5}$$

The study aims to fabricate vertically-oriented SiNWs and to attain control of the geometry and crystallinity of these nanostructures by varying the etching parameters. The effect of each parameter was observed using different characterization tools. The dimensions of the NWs were examined and measured using a Scanning Electron Microscope (SEM). X-ray diffractometry (XRD) was used to determine any changes in the quality of the crystal structures in the Si substrate. Raman spectroscopy was performed to determine whether the etched SiNWs retained their crystallinity. Photoluminescence (PL) spectroscopy was used to determine the possible radiative transitions of the SiNWs.

METHODOLOGY

A monocrystalline p-type Si (100) wafer with a resistivity of 0.3-300Ω•cm and thickness of 500 µm was used as a substrate. The wafer was cleaned using standard degreasing procedures. It was then immersed in a solution of 48% HF and DI water (1:9 volumetric ratio) to remove the oxides formed at the surface. The surface was cleaved into 1 cm × 1 cm samples, upon which the NWs were etched.

For the one-step standard etching, Ag deposition and etching was achieved through the immersion of the substrate in a solution of 5.0 M HF and 0.02 M AgNO$_3$ for 60 minutes. Each substrate was rinsed with DI water after etching. The Ag dendrites formed at the surface of the sample after immersion (representative image in the Supplementary Material) were carefully removed using tweezers, and the remaining Ag particles on the samples were chemically removed using a solution of NH$_4$OH and H$_2$O$_2$ at a 3:1 volumetric ratio.

For two-step standard etching, Ag deposition was performed through the immersion of the samples in an etchant solution of 5.0 M HF and 0.02 M AgNO$_3$ for 2 minutes. The samples were then rinsed with DI water to remove loose Ag particles and excess ions from the etchant solution. To etch the NWs, the samples were immersed in a solution of 5.0 M HF and 0.3 M H$_2$O$_2$ for 40 minutes. The samples were again washed with DI water after the etching. The deposited Ag particles were removed in the samples via immersion in a solution of NH$_4$OH and H$_2$O$_2$ with a 3:1 volumetric ratio.

For the one-step etching process, AgNO$_3$ concentration was varied from 0.01 to 0.04 M, HF concentration from 2.5 to 7.5 M, and the etch time between 120 and 180 minutes. For the two-step etching Ag deposition, the deposition time was varied from 1 to 3 minutes, HF concentration from 2.5 to 7.5 M, H$_2$O$_2$ concentration from 0.1 to 0.5 M, and the etch time to 120 and 180 minutes. The concentrations of the chemicals, Ag deposition time, and etch time are summarized in Tables 1 and 2. Only one parameter was changed from the standard procedure per sample, in order to determine the individual effects of the parameters on the SiNW structure.

Table 1. The modified parameters (highlighted) in the one-step etching process. The first row of parameters is the standard used by Peng et al. (2002)

HF Concentration (M)	AgNO$_3$ Concentration (M)	Etch Time (minutes)
5.0	0.02	60
2.5	0.02	60
7.5	0.02	60
5.0	0.01	60
5.0	0.04	60
5.0	0.02	120
5.0	0.02	180

Table 2. The modified parameters (highlighted) in the two-step etching process. The first row of parameters is the standard used by Peng et al. (2002)

Ag Deposition Time (seconds)	HF Concentration (M)	H$_2$O$_2$ Concentration (M)	Etch Time (minutes)
120	5.0	0.3	40
60	5.0	0.3	40
180	5.0	0.3	40
120	2.5	0.3	40
120	7.5	0.3	40
120	5.0	0.1	40
120	5.0	0.5	40
120	5.0	0.3	20
120	5.0	0.3	60

SiNW images were captured using a Philips XL-30 FEG SEM. Measurements from the images were obtained using SEM software's built-in measurement application, along with an external application TSView. The XRD pattern was obtained using a Bede D3 High Resolution X-Ray Diffractometer. The wavelength of the incident X-ray from a Cu Kα source was 1.541 Å, and the scan resolution was 0.002°. Raman spectroscopy was performed with an excitation provided by a 60-mW, 514.5-nm Ar$^+$ laser, and the scan resolution was 1.2 cm^{-1}. The scattered light was detected by a Horiba Jobin-Yvon iHR 550 imaging spectrometer with a charge-coupled device (CCD) detector. PL was executed with an excitation provided by a 488-nm Ar$^+$ laser, and the detection apparatus was a SPEX 500M equipped with a photomultiplier tube.

RESULTS AND DISCUSSION

One-step Etching

Dependence on HF concentration

The SEM image in Figure 2 shows that the increase in HF concentration was directly proportional with the length of the SiNWs. Following the implementation of the Nernst equation on reactions (1), (2), (3) by Lin et al. (2010), the potential of the one-step etching process is governed by:

$$\Delta E = \Delta E^0 - \frac{0.059}{4} \log \frac{[SiF_6^{2-}]}{[Ag^+]^4[F^-]^6} \tag{6}$$

From the equation (6), an increase in concentration of the HF directly affects the amount of free F$^-$ ions. Thus, we should see an increase in the electric field produced by the etching process. F$^-$ theoretically has the highest contribution to the electric field process.
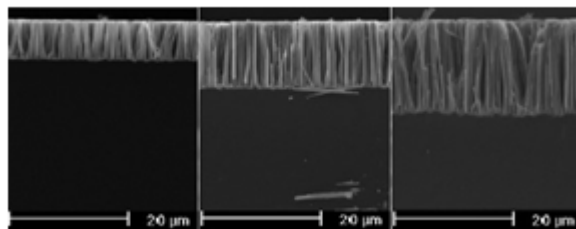
Figure 2. SEM micrographs showing increasing lengths of SiNWs (8, 13, and 19 ìm) as HF concentration was increased (2.5, 5.0, and 7.5 M) (left to right).

The increase in length of the nanowires consequently results to the agglomeration at the tips of the nanowires. This agglomeration results from van der Waals forces (Li et al. 2010) and capillary forces due to water (Choi et al. 2010). By lengthening the SiNWs, the elastic deformation force (F_{ed}), which counters the bending forces from the van der Waals and its capillary effect, becomes weak (Togonal et al. 2014). The weakening of the elastic deformation is given by the following equation:

$$F_{ed} = \frac{(3\pi ER^4)}{4L^3}$$ (7),

where E is the Young's modulus, L is the length of the nanowires, and R is the radius of the nanowires.

The HF concentration has no significant effect to the diameter or to the nanowire density as shown in Table 3.

Dependence on AgNO$_3$ Concentration

From equation (6), the Ag+ contribution is only raised to 4, but the increment in the AgNO$_3$ molarity increased by 2.0× (from 0.02 to 0.04 M), while the HF molarity increased by 1.5× (from 5 to 7.5 M). Hence, changing the AgNO$_3$ concentration has a larger contribution to the increase in nanowire length.

The SEM image in Figure 3 shows that an increase in AgNO$_3$ concentration also enhanced the length of the SiNWs. This observation can be attributed to the increase in the hole sources being injected to the silicon substrate. From the coupled equations (1) and (2), more Ag+ extract electrons from the silicon surface, which eventually becomes Ag(s) and simultaneously oxidizes silicon. The increase in Ag+ ions does not only cause an increase in the amount of Ag deposited at the surface of
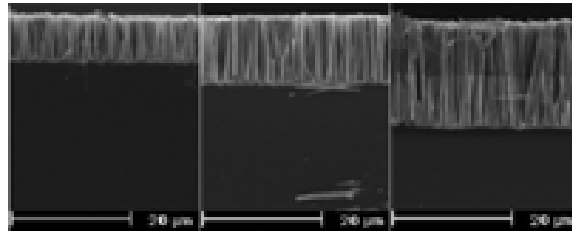
Figure 3. SEM micrographs showing increasing lengths of SiNWs (10, 13, and 21 µm) as AgNO$_3$ concentration was increased (0.01, 0.02, and 0.04 M) (left to right).

the silicon but also the surface area available for etching. Consequently, this caused an increase in the nanowire density (Table 3).

Table 3. Summary of the measurements and characterizations of the SiNW samples produced with varying parameters in the one-step etching process

HF Conc. (M)	AgNO₃ Conc. (M)	Etch Time (minutes)	NW Length (μm)	NW Diameter (nm)	NW count Density (no./μm²)	XRD Peak (⁰)	XRD FWHM	Raman Peak (cm⁻¹)
-	-	-	-	-	-	69.112	0.012	520.0
5.0	0.02	60	12.8 ± 0.3	170 ± 122	44	69.112	0.012	517.4
2.5	0.02	60	7.9 ± 0.3	99 ± 39	131	69.112	0.024	517.8
7.5	0.02	60	19.3 ± 1.0	122 ± 62	86	69.112	0.027	518.0
5.0	0.01	60	9.8 ± 0.3	137 ± 98	68	69.112	0.010	517.5
5.0	0.04	60	21.4 ± 1.0	120 ± 48	88	69.112	0.008	516.4
5.0	0.02	120	30.8 ± 0.9	157 ± 104	52	69.112	0.030	515.6
5.0	0.02	180	37.2 ± 2.5	172 ± 88	43	69.112	0.046	515.5

Dependence on etch time

The SEM image in Figure 4 shows that the increase in the etch time also caused an increase in the length of the SiNWs. The increase in etch time allows the reactions to proceed, and as a result, the AgNPs burrow more deeply into the substrate. The increase in the length of the nanowire results to the agglomeration at their tips. The top-view SEM in Figure 5 shows the formation of distinctive clusters of NWs as the SiNW length increased. There is an observed increase in the nanowire diameter for the 180-minute etch.
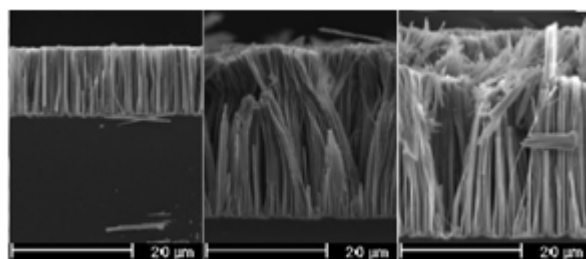
Figure 4. SEM micrographs showing increasing lengths of SiNWs (13, 31, and 37 ìm) as etch time was increased (60, 120, and 180 minutes) (left to right).
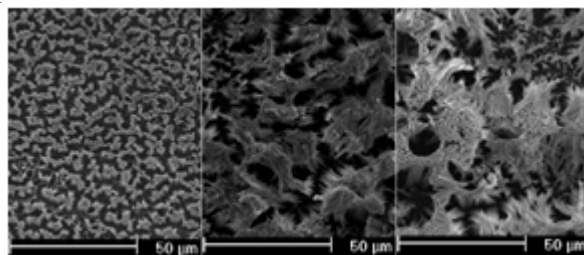
Figure 5. Top-view SEM micrographs of the samples as etch time was increased (60, 120, and 180 minutes). The degree of agglomeration or the clustering at the tips of the NWs increased as the SiNW length increased.

The XRD plot from Figure 6 reveals that, as the etch time was increased, the full-width at half-maximum (FWHM) also exhibited a slightly increasing trend. The samples demonstrated a somewhat lower crystal quality, as can be observed from their broadened XRD peaks. Moreover, compared to the FWHM of bulk Si, the samples displayed degradation in the crystal quality after etching SiNWs to the samples, which can be a consequence of non-uniform surface stress encountered by the nanowire (Song et al. 2011).

The Raman spectroscopy plot shown in Figure 7 confirms that the SiNWs are indeed crystalline. The SiNW Raman peaks are downshifted relative to the bulk Raman peaks, but this is not a result of phonon confinement because the maximum diameter for nanowires to exhibit quantum confinement is at 20 nm (Richter et al. 1981;
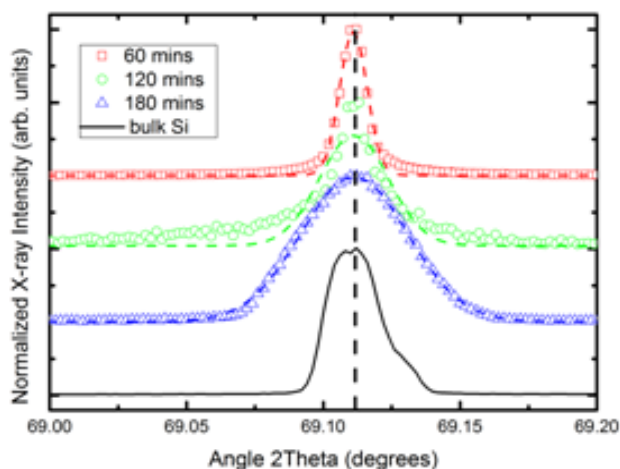
Figure 6. XRD peaks of one-step electroless etching SiNWs as etch time was increased (60, 120, and 180 minutes).

Campbell and Fauchet 1986). Instead, this can be ascribed to laser heating as a consequence of subjecting the SiNWs to a high-power laser in the Raman set-up, a phenomenon encountered by Scheel et al. (2008). The dissipation of heat in SiNWs is efficient only along one direction, which makes SiNWs excellent thermo-insulators. The down-shifting is different for each sample due to the non-linear relationship between thermal conductivity and SiNW length (Wang et al. 2012).
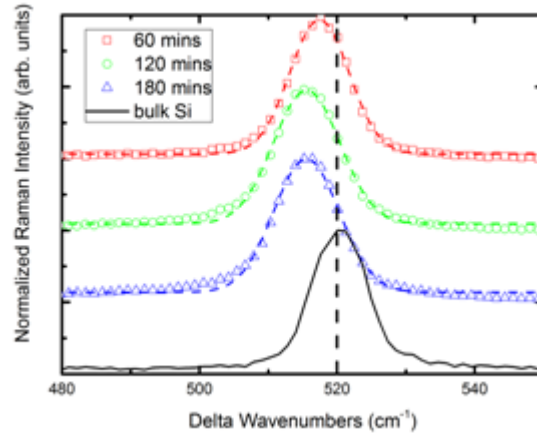
Figure 7. Raman peaks for one-step electroless etching SiNWs as etch time was increased (60, 120, and 180 minutes). A downshift from the bulk Si peak (solid line) is observed for all SiNW samples.

Two-step Etching

Dependence on the Ag deposition time

For the two-step process, the potential for the etching process from the Nernst equation (Lin et al. 2010) becomes:

$$\Delta E = \Delta E^0 - \frac{0.059}{4} \log \frac{[SiF_6^{2-}]}{[H_2O_2]^2 [H^+]^4 [F^-]^6} \tag{8}$$

Thus, theoretically, Ag deposition should be independent of the etching process.

At low deposition times, little agglomeration occurred at the tip of the NWs (Figure 8). Meanwhile, the mean diameter of NWs decreased as deposition time increased (Figure 8). This can be attributed to the increase in the area covered by the deposited

Ag as the deposition time increased. Because the unetched area decreased, then the diameters of the NWs formed in the process also decreased. There was a slight increase in the etch depth as the deposition time increased (Figure 9). Longer deposition time yielded increased area covered by Ag deposition on the surface of Si, resulting to better electron capture from the electrolyte. As a consequence, the SiNW density increased while the aspect ratio did not exhibit a clear trend.
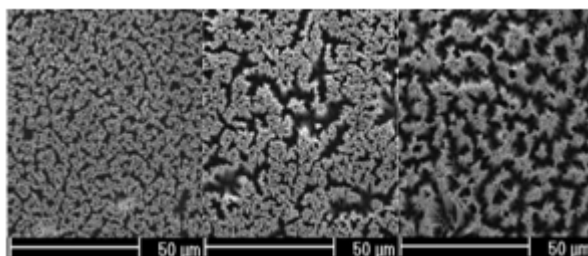
Figure 8. Top-view SEM micrographs of the samples showing the agglomeration of SiNW tips as Ag deposition time was increased (60, 120, and 180 seconds).
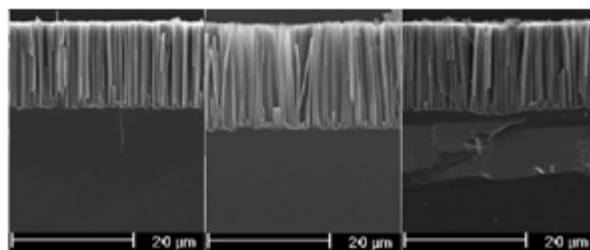
Figure 9. SEM micrographs showing independence of the length of SiNWs (16, 19, and 16 ìm) on increasing Ag deposition time (60, 120, and 180 seconds) (left to right).

Dependence on HF concentration

From the Nernst equation (8), HF has the highest contributing factor, as demonstrated by the 29-μm length of SiNWs etched.

The etch depth increased as the concentration of HF increased (Figure 10). Meanwhile, the mean diameter (Table 3) of SiNWs decreased with increasing HF concentration. Such trend is attributed to the faster anisotropic etching along the direction of Ag particles, as well at the sidewalls of SiNWs, due to the large amount of HF available to etch the oxidized Si. Thus, increasing the HF concentration resulted to a great increase in the density and aspect ratio of SiNWs.
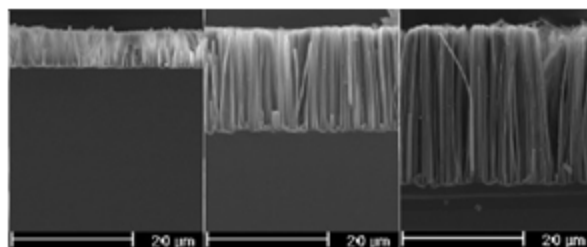
Figure 10. SEM micrographs showing increasing lengths of SiNWs (7, 19, and 29 ìm) as HF concentration was increased (2.5, 5.0, and 7.5 M) (left to right).

Dependence on H$_2$O$_2$ concentration

At low H$_2$O$_2$ concentrations, AgNPs catalyze with just the small amount of H$_2$O$_2$, thereby exhausting the H$_2$O$_2$ supply. With increasing H$_2$O$_2$ supply, the process of AgNO$_3$ is hastened and greater etch depth is observed. However, at higher concentrations (0.5 M H$_2$O$_2$), the length of SiNWs decreased. As described by Li et al. (2014), an increase in H$_2$O$_2$ concentration leads to horizontal and vertical etching on the silicon nanowire (Figure 11).

Dependence on etch time

Similar to the one-step etch, the increase in the etch time also caused an increase in the length of the SiNWs (Figure 12). The degree of agglomeration of the nanowires increased as the time of etching increased, similar to what is observed in the one-step etching (Figure 13). No change was observed in the diameter or the density of the nanowires as the etch time increased (Table 4).
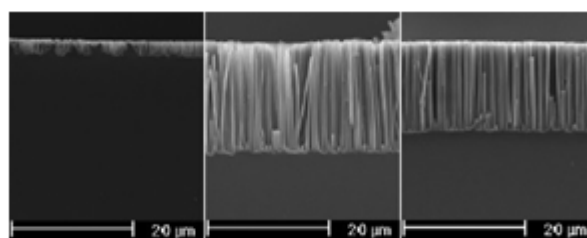
Figure 11. SEM micrographs showing varying SiNW lengths (2, 19, and 16 ìm) as H$_2$O$_2$ concentration was increased (0.01, 0.02, and 0.04 M) (left to right).

From the XRD data summarized in Table 4, no clear trend was observed in the crystal quality of the samples. The samples were crystalline; however, they possessed lower crystal quality compared to bulk Si, as suggested by their broadened peaks in Figure 14. The decrease in crystal quality can be attributed to the surface roughness of the SiNWs brought about by the etching step in the two-step process.

There are two salient features in the Raman spectrum for all two-step etched SiNWs, a broad peak and a sharp peak. The sharp peak is attributed to the crystalline Si (c-Si), and the broad peak is imputed to the contributions of lower energy phonon modes due to the porous sidewalls. Table 3 shows both sharp and broad peaks.

Table 4. Summary of the measurements and characterizations of the SiNW samples produced with varying parameters in the two-step etching process

Ag Deposition Time (seconds)	HF Conc. (M)	H_2O^2 Conc. (M)	Etch Time (mins.)	NW Length (µm)	NW Diameter (nm)	NW couynt Density (no./ (µm²)	XRD Peak (°)	XRD FWHM	Raman Peak 1 (sharp) and Peak 2 (broad) (cm⁻¹)	
-	-	-	-	-	-	-	69.112	0.012	520.0	-
120	5.0	0.3	40	19.3 ± 0.5	193 ±108	34	69.112	0.033	514.0	489.9
60	5.0	0.3	40	15.7 ± 0.4	210 ±135	28	69.112	0.035	513.3	496.7
180	5.0	0.3	40	16.4 ± 0.3	166 ± 92	46	69.112	0.045	516.1	504.0
120	2.5	0.3	40	7.3 ± 0.4	164 ± 90	47	69.112	0.045	517.8	502.3
120	7.5	0.3	40	28.9 ± 0.9	154 ± 73	53	69.112	0.038	515.7	500.3
120	5.0	0.1	40	2.3 ± 0.7	80 ± 57	198	69.112	0.036	519.2	———
120	5.0	0.5	40	15.7 ± 0.4	189 ± 99	36	69.112	0.056	512.9	488.7
120	5.0	0.3	20	11.0 ± 0.5	172 ±106	43	69.112	0.056	519.0	505.5
120	5.0	0.3	60	26.0 ± 0.8	197 ± 90	33	69.112	0.049	513.5	496.2
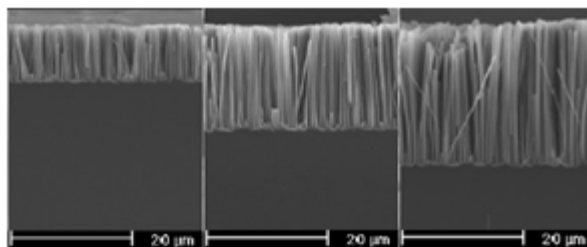
Figure 12. SEM micrographs showing increasing lengths of SiNWs (11, 19, and 26µm) as etch time was increased (20, 40, and 60 minutes) (left to right).
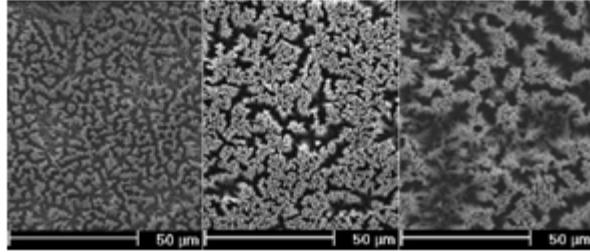
Figure 13. Top-view SEM micrographs of the samples as etch time was increased (20, 40, and 60 minutes). The degree of agglomeration or the clustering at the tips of the SiNWs increased as the SiNW length increased.
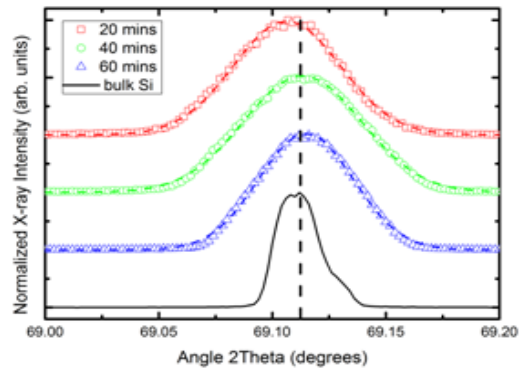
Figure 14. XRD peaks of two-step electroless etching SiNWs as etch time was increased (20, 40, and 60 minutes). There was no apparent shift from the peak of bulk Si (solid line). No trend was observed on the FWHM.
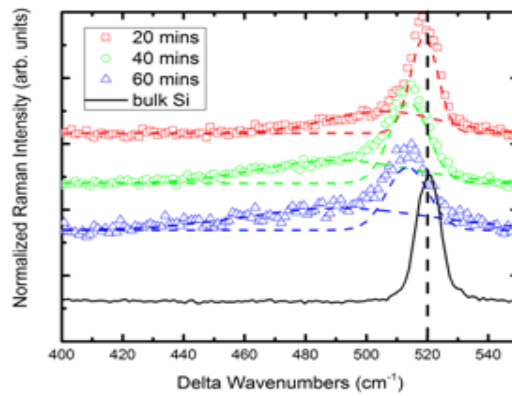
Figure 15. Raman peaks for the bulk Si and the two-step electroless etching SiNWs as etch time was increased (20, 40, and 60 minutes). Broad and sharp peaks were observed in the SiNW plots.

Photoluminescence (PL) Spectra of SiNWs

Analyses based solely on intensities of the PL peaks reveal insufficient information on the possible radiative transitions of the SiNWs. In reality, these PL peaks are just a sum of several Gaussian peaks from unique defects (Muldera et al. 2013; Ghosh et al. 2014). To gain more information from the PL peaks for both the one-step and the two-step electroless etching, each peak was deconvolved to four Gaussian peaks centering at approximately 590 nm, 663 nm, 759.9 nm, and 850 nm. The 590-nm peak can be attributed to the defects from Si-Si dimer, which is commonly known as the host dioxide matrix (HDM) by Kamenev and Nassiopoulou (2010). This peak is intrinsic to silicon nanowires. As observed by Najar et al. (2012), the 663-nm peak comes from the oxygen defect of Si. The two PL peaks which approximately lie at 760 nm and 850 nm can be assigned to two unique oxide surface defects (Lin 2010). The ratios of the area under the curve of these four Gaussian peaks were obtained with respect to the area under the fitted plot. The areas under the curve of the fitted plot were obtained using Simpson's rule. Figure 16 and 17 show the deconvolution of the PL peaks and their ratios in percent using a Peak Fit program.

Peaks 3 and 4 are the oxide surface defects which come from the oxide dangling defects in the oxide layer of the silicon (Lin et al. 2010).
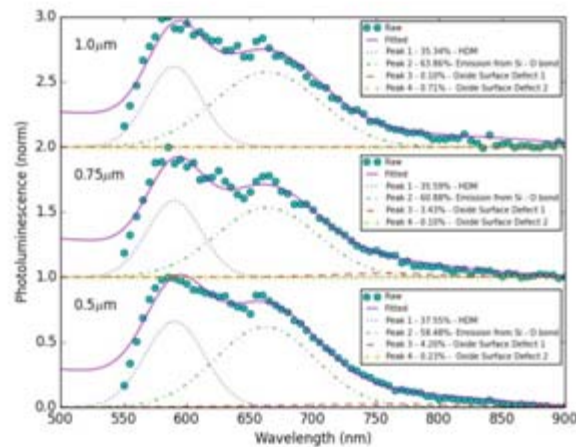
Figure 16. PL intensity of increasing lengths of one-step electroless etching SiNWs (0.5, 0.75, and 1.0 µm), with each peak deconvolved into four Gaussian peaks.
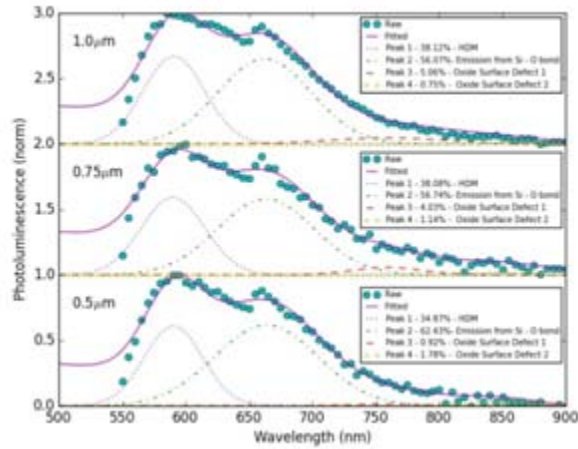
Figure 17. PL intensity of increasing lengths of one-step electroless etching SiNWs (0.5, 0.75, and 1.0 m), with each peak deconvolved into four Gaussian peaks.

The area under the curve ratios for one-step and two-step etching processes are listed in Tables 5 and 6, respectively.

As the HDM (590 nm) defect increased, the defect from the Si-O bond (663 nm) decreased, suggesting an inverse relationship between the two defects. This inverse relationship between the two defects was observed in both one-step and two-step processes with increasing nanowire length. For the two other oxide surface defects (759 nm and 850 nm), the values were too small (<5% of the actual intensity) to show any trend. PL due to quantum confinement is also negligible due to the large diameters of the SiNWs formed.

Table 5. Area under the curve PL values in % for the one-step electroless etching process

SiNW length (μm)	590.5 nm	663 nm	760 nm	590.5 nm
0.5 μm	37.55 %	58.48 %	4.20 %	0.23%
0.75 μm	35.59 %	60.88 %	3.43 %	0.1 %
1.0 μm	35.35 %	63.86 %	0.1 %	0.71 %

**Table 6. Area under the curve PL values in % for the
two-step electroless etching process**

SiNW length (µm)	593 nm	663 nm	760 nm	850 nm
0.5 µm	34.87 %	62.43 %	0.92 %	1.78%
0.75 µm	38.08 %	56.74 %	4.03 %	1.14 %
1.0 µm	38.12 %	56.07 %	5.06 %	0.75 %

CONCLUSION

As the parametric values were increased, the wire lengths also increased, with etch time being the most significant factor, followed by $AgNO_3$ and HF concentration. The uniformity of the nanowire diameter can be modified by the $AgNO_3$ concentration. Increasing the H_2O_2 concentration of the second etchant caused a decrease in the nanowire diameter. From the XRD analysis of the one-step etching, the crystallinity of the SiNWs was slightly compromised with increasing parametric values. However, for the two-step etching, no clear trend was observed. The broadening and downshifting of the SiNW's Raman spectra relative to the bulk Si can be attributed to laser heating and the low thermal conductivity of the SiNWs. The photoluminescence of the SiNWs were obtained as well, relating the area under the curve plots of the deconvolved Gaussian peaks to their corresponding defects. An inverse relationship was observed for the host dioxide matrix defect and the Si-O bond defect.

ACKNOWLEDGMENTS

REFERENCES

Bandaru P, Pichanusakorn P. 2010. An outline of the synthesis and properties of silicon nanowires. Semiconductor Science and Technology. 25(2):024003.

Campbell I, Fauchet P. 1986. The effects of microcrystal size and shape on the one phonon raman spectra of crystalline semiconductors. Solid State Communications. 58(10):39-741.

Choi C, Yoon Y, Hong D, Jin S. 2010. Strongly superhydrophobic silicon nanowires by supercritical CO2 drying. Electronic Materials Letters. 6(2):59-64.

Curtin B, Fang E, Bowers J. 2012. Highly ordered vertical silicon nanowire array composite thin films for thermoelectric devices. Journal of Electronic Materials. 41(5):887-894.

Gunawan O, Guha S. 2009. Characteristics of vapor-liquid-solid grown silicon nanowire solar cells. Solar Energy Materials and Solar Cells. 95(1):1388-1393.

Ghosh R, Giri PK, Imakita K, Fujii M. 2014. Origin of visible and near-infrared photoluminescence from chemically etched Si nanowires decorated with arbitrarily shaped Si nanocrystals. Nanotechnology. 25(4):045703.

Kamenev BV, Nassiopoulou AG. 2001. Self-trapped excitons in silicon nanocrystals with sizes below 1.5 nm in Si/SiO2 multilayers. Journal of Applied Physics. 90(11):5735-5740.

Li C, Fang G, Sheng S, Chen Z, Wang J, Ma S, Zhao X. 2005. Raman spectroscopy and field electron emission properties of aligned silicon nanowire arrays. Physica E: Low-dimensional Systems and Nanostructures. 30(1):169-173.

Li S, Ma W, Zhou Y, Chen X, Xiao Y, Ma M, Zhu W, Wei F. 2014. Fabrication of porous silicon nanowires by MACE method in $HF/H_2O_2/AgNO_3$ system at room temperature. Nanoscale Research Letters. 9(1):196.

Lin L, Guo S, Sun X, Feng J, Wang Y. 2010. Synthesis and Photoluminescence Properties of Porous Silicon Nanowire Arrays. Nanoscale Research Letters. 5(11):1822-1828.

Liu K, Qu S, Zhang X, Tan F, Wang Z. 2013. Improved photovoltaic performance of silicon nanowire/organic hybrid solar cells by incorporating silver nanoparticles. Nanoscale Research Letters. 8(1):88.

Muldera J, Cabello N, Ragasa JC, Mabilangan A, Balgos MH, Jaculbia R, Somintac A, Estacio E, Salvador A. 2013. Photocarrier transport and carrier recombination efficiency in vertically aligned Si nanowire arrays synthesized via metal-assisted chemical etching. Applied Physics Express. 6(8):082101.

Najar A, Dalaver AH, Hedhili MN, Ng TK, Ooi BS, Slimane AB, Sougrat R. 2012. Effect of hydrofluoric acid concentration on the evolution of photoluminescence characteristics in porous silicon nanowires prepared by Ag-assisted electroless etching method. Journal of Applied Physics. 112(3):033502.

Pan H, Chen W, Lim SH, Poh CK, Wu X, Feng Y, Ji W, Lin J. 2005. Photoluminescence and optical limiting properties of silicon nanowires. Journal of Nanoscience and Nanotechnology. 5(5):733-737.

Peng K, Yan Y, Gao S, Zhu J. 2002. Synthesis of large-area silicon nanowire arrays via self-assembling nanoelectrochemistry. Advanced Materials. 14(16):1164-1167.

Peng KQ, Hu JJ, Yan YJ, Wu Y, Fang H, Xu Y, Lee S, Zhu J. 2006. Fabrication of single-crystalline silicon nanowires by scratching a silicon surface with catalytic metal particles. Advanced Functional Materials. 16(3):387-394.

Richter H, Wang Z, Ley L. 1981. The one phonon Raman spectrum in microcrystalline silicon. Solid State Communications. 39(5):625-629.

Scheel H, Khachadorian S, Cantoro M, Colli A, Ferrari AC, Thomsen C. 2008. Silicon nanowire optical Raman line shapes at cryogenic and elevated temperatures. Physica Status Solidi b. 245(10):2090-2093.

Schmidt V, Wittemann JB, Senz S, Gösele U. 2009. Silicon nanowires: A review on aspects of their growth and their electrical properties. Advanced Materials. 21(25-26):2681-2702.

Song F, Huang GL, Park HS, Liu XN. 2011. A continuum model for the mechanical behavior of nanowires including surface and surface-induced initial stresses. International Journal of Solids and Structures. 48(14-15):2154-2163.

Togonal AS, He L, and Roca iCabarrocas P. 2014. Effect of wettability on the agglomeration of silicon nanowire arrays fabricated by metal-assisted chemical etching. Langmuir. 30(34):10290-10298.

Tsakalakos L, Balch J, Fronheiser J, Shih MY, LeBoeuf SF, Pietrzykowski M, Codella PJ, Korevaar BA, Sulima O, Rand J, Davuluru A. 2007. Strong broadband optical absorption in silicon nanowire films. Journal of Nanophotonics. 1(1):013552.

Wang Y, Schmidt V, Senz S, Gösele U. 2006. Epitaxial growth of silicon nanowires using an aluminum catalyst. Nature Nanotechnology. 1(3):186-189.

Wang M, Shan X, and Yang N. 2012. Understanding length dependences of effective thermal conductivity of nanowires. Physics Letters A. 376(46):3514-3517.

_____

Neil Irvin F. Cabello graduated B.S. Applied Physics (Instrumentation) and M.S. Physics from the University of the Philippines Diliman. He is currently a Ph.D. Physics student at the University of the Philippines Diliman and a Research Fellow in the CHEF-PCARI project "3V-ReCoN." His research interests include silicon nanowires and porous Silicon (pSi) application, photoluminescence and THz applications of these nanostructures, and vertical cavity surface emitting lasers (VCSELs).

Eloise P. Anguluan graduated B.S. Applied Physics (Instrumentation) and M.S. Physics from the University of the Philippines Diliman. She is currently a researcher in Gwangju Institute of Science and Technology, South Korea. Her research interests include electro-optical characterization of pSi and SiNWs, enhanced Raman Spectroscopy, and biophotonics.

Joseph Christopher R. Ragasa graduated B.S. Physics from the University of the Philippines Diliman. He is currently employed in HGST company. His research interests include SiNWs fabrication, harvest, and application for optoelectronic devices.

Philippe Martin B. Tingzon <ptingzon@gmail.com> graduated B.S. Applied Physics (Instrumentation) and M.S. Materials Science and Engineering from the University of the Philippines Diliman. He is currently a Ph.D. Materials Science and Engineering student at the University of the Philippines and a Research Fellow in the CHEF-PCARI project "3V-ReCoN". His research interests include silicon nanowires applications, GaAs-based solar cells, and vertical cavity surface emitting lasers (VCSELs).

Kerr A. Cervantes is currently an undergraduate student taking up B.S. Applied Physics (Materials Physics) at the University of the Philippines Diliman. His research interests include SiNWs fabrication and application.

Arvin Jay S. Escolano graduated B.S. Applied Physics (Materials Physics) and is currently taking up M.S. in Materials Science and Engineering at the University of the Philippines Diliman. He is currently a DOST scholar under the DOST-ASTHRD program. His research interests include SiNWs fabrication and application, and SnO_2/Fe_2O_3 pyroelectric films.

Dr. Arnel A. Salvador graduated B.S. Physics from the University of the Philippines Diliman and Ph.D. in Physics from University of Illinois. He is currently a Professor at the National Institute of Physics and the Chairperson of the Physics Division of the National Research Council of the Philippines. His research specialization include MBE (Molecular Beam Epitaxy) grown nanostructures with their corresponding properties and applications such as VCSELs.

Dr. Armando S. Somintac graduated B.S. Physics in the University of the Philippines Baguio as his undergraduate course, took his MS in Materials Science and Engineering from the University of the Philippines Diliman and finished his Ph.D. in Physics from the same university. He is currently a Professor at the National Institute of Physics and the Director of the Project Management and Resource Generation Office of the Office of the Vice-Chancellor for Research and Development. His research specializations include nano-structured semi-conductors for devices and sensors.